East European Journal of Physics. 1. 250-255 (2025)
DOI:10.26565/2312-4334-2025-1-27 ISSN 2312-4334

OPTICAL PERFORMANCE AND CRYSTAL STRUCTURE OF TiO_2 THIN FILM ON GLASS SUBSTRATE GROWN BY ATOMIC LAYER DEPOSITION

Temur K. Turdaliev
Arifov Institute of Ion-Plasma and Laser Technologies of Uzbekistan Academy of Sciences
100125, Durmon Yuli st. 33, Tashkent, Uzbekistan
Corresponding Author e-mail: turdaliev@iplt.uz
Received September 9, 2024; January 16, 2025; accepted January 20, 2025

This study investigates the formation of the optical properties and crystal structure of TiO_2 thin films, with a thickness of approximately 1.5 micrometers, grown on a glass substrate using the atomic layer deposition method with titanium tetraisopropoxide and water as precursors. X-ray diffraction and Raman spectroscopy analyses confirmed that the TiO_2 films crystallize in the anatase polymorphic phase. The films exhibit a nanocrystalline structure with an average crystallite size of approximately 28 nanometers, as established by X-ray diffraction measurements. The X-ray diffraction pattern revealed distinct peaks at 2θ angles of 25.3°, 38.6°, 48.0°, 55.0°, and 70.4°, corresponding to the (101), (112), (020), (121), and (220) crystallographic planes, while the Raman spectra exhibited pronounced peaks at frequencies of 143, 194, 392, 514, and 637 cm^{-1}, all characteristic of the anatase phase of TiO_2. The Tauc method applied to the absorption spectra of the thin film showed that it has a direct bandgap of 3.2 eV and an indirect bandgap of 2.3 eV.
Keywords: *Titanium dioxide thin films; Atomic layer deposition; Anatase phase; X-ray diffraction; Raman spectroscopy; Bandgap energy; Optical properties; Urbach energy; Nanocrystalline structure*
PACS: 78.66.-w, 68.55.Jk, 78.30.-j, 73.61.Ng

INTRODUCTION

In recent years, there has been significant interest in TiO_2 due to its unique properties, including high chemical stability, low toxicity, and a variety of structural phases [1–3]. One of the key features of TiO_2 is its ability to actively absorb ultraviolet radiation while remaining transparent in the visible spectrum, making it an ideal material for optoelectronic applications. The optical properties of TiO_2 are determined by its crystalline phase, particle size, and the presence of defects, which can affect light transmission and absorption [4, 5]. The bandgap width of TiO_2 varies depending on the synthesis method and ranges from 2.6 to 3.3 eV [6, 7]. Due to these characteristics, the material is promising for the creation of optoelectronic devices. In particular, the optical properties of TiO_2 allow for enhanced light absorption in solar cells, which improves energy conversion efficiency [8]. Additionally, its application as a material for heterojunction solar cells opens up further possibilities for the development of highly efficient photovoltaic systems [9]. In addition to solar cells, TiO_2 thin films have found widespread applications in a range of advanced technologies. TiO_2 films are also extensively can used in self-cleaning surfaces due to their photocatalytic activity, where under ultraviolet light, they can break down organic contaminants, making them ideal for use in building materials, glass coatings, and environmental purification [10, 11]. Moreover, TiO_2 thin films serve as efficient dielectric layers in capacitors and as gate insulators in field-effect transistors due to their excellent insulating properties [12]. In gas sensor technology, the sensitivity of TiO_2 to various gases, such as hydrogen, makes it a valuable material for detecting pollutants and hazardous gases in the environment [13]. Another promising application is in photocatalytic water splitting for hydrogen production, where TiO_2 acts as a photoanode, contributing to sustainable energy solutions. Thin TiO_2 films can also be used as buffer layers, particularly for the catalytic growth of carbon nanotubes [14, 15]. The combination of optical transparency, photocatalytic activity, and chemical stability also makes TiO_2 thin films suitable for use in medical devices and antibacterial coatings, adding to their versatility across multiple industries.

There are numerous methods for obtaining thin films of TiO_2, including the sol-gel method [6], reactive magnetron sputtering [16], solvothermal synthesis [17, 18], and atomic layer deposition (ALD) [19]. These methods make it possible to form films with various morphologies, ranging from nanoparticles [20] to nanotubes [21, 22] and nanorods [23], allowing the material's properties to be adapted to specific tasks depending on the field of application.

In this work, we study the features of the formation of optical properties and the crystalline structure of a titanium dioxide thin film obtained by the ALD method using titanium tetraisopropoxide (TTIP) and water as precursors. A comprehensive structural analysis was carried out, as well as an investigation of the film's optical properties using absorption spectroscopy at room temperature.

EXPERIMENT

TiO_2 was deposited onto a pre-prepared glass substrate using the thermal ALD method on an SI PEALD system (SENTECH Instruments GmbH). During the deposition process, TTIP and water were used as the primary precursors, while nitrogen was employed as both the carrier and purging gas.

Cire as: T.K. Turdaliev, East Eur. J. Phys. 1, 250 (2025), https://doi.org/10.26565/2312-4334-2025-1-27

The deposition parameters were as follows: nitrogen flow rate was 120 cm³/min, reactor pressure was approximately 60 Pa, substrate temperature was around 225°C, and each cycle duration was 8 seconds. The process consisted of 5 steps in the following sequence: an initial purge; introduction of TTIP for 0.5 seconds; nitrogen purging for 3 seconds; introduction of H_2O for 1.5 seconds; and final nitrogen purging for 3 seconds. Under these conditions, the growth rate per cycle was 0.2 nm, and the deposition process was carried out for 7500 cycles. As a result, a sample with a TiO_2 film thickness of 1500 nm was obtained. A visual representation of the titanium dioxide film deposition process by the ALD method is shown in Figure 1.

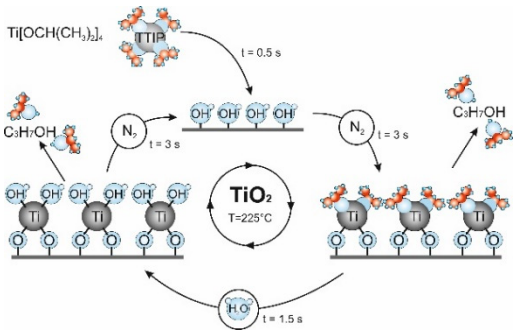

Figure 1. Schematic diagram of the ALD process of TiO_2 on a glass substrate

XRD Structural Analysis

TiO_2 can exist in three crystalline forms: the stable rutile phase and two metastable phases—anatase and brookite [3]. Both rutile and anatase have a tetragonal structure but differ in lattice parameters and space groups. Rutile is more stable at high temperatures, whereas anatase and brookite form at lower temperatures and transform into rutile upon heating. Each of these phases possesses unique optical and structural characteristics, making them suitable for various technological applications.

X-ray diffraction analysis of the samples was carried out using a PANalytical Empyrean diffractometer, confirming the formation of the TiO_2 film in the anatase polymorph after the deposition process. As shown in Figure 2, the diffraction pattern of the freshly deposited sample exhibits clear peaks characteristic of the anatase phase of TiO_2 at 2θ angles: 25.3°, 38.6°, 48.0°, 55.0°, and 70.4°, corresponding to the (101), (112), (020), (121), and (220) crystallographic planes of anatase. Additionally, no reflections characteristic of other TiO_2 polymorphs, such as rutile or brookite, were observed, confirming the purity of the anatase phase [6, 24].

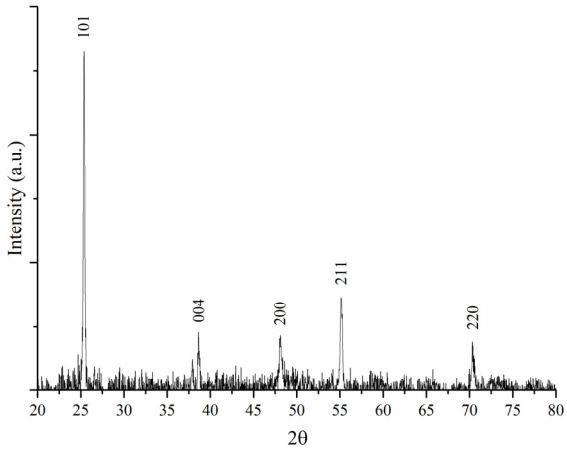

Figure 2. X-ray diffraction pattern of the TiO_2 film. Characteristic reflections for the anatase phase of titanium dioxide are observed at 2θ angles: 25.3° (101), 38.6° (004), 48.0° (200), 55.0° (211), and 70.4° (220)

The interplanar spacing of the crystal (d) was calculated based on the obtained diffraction patterns using Bragg's equation [6]:

$$d = \frac{n\lambda}{2sin\theta} \tag{1}$$

where d is the interplanar spacing between atomic planes, n = 1 is the order of diffraction, λ = 1.5406 Å represents the wavelength for CuKα radiation, and θ is the diffraction angle.

The obtained d values were subsequently used to calculate the crystal lattice parameters. For the tetragonal structure, the lattice parameters a and c were determined using the following equation:

$$\frac{1}{d^2} = \frac{h^2+k^2}{a^2} + \frac{l^2}{c^2} \tag{2}$$

h, k, and *l* are the Miller indices for the corresponding crystallographic planes, and *a* and *c* are the lattice parameters. The calculated lattice parameters were a = 0.3785 nm and c = 0.9513 nm, which are in agreement with the literature values for the anatase phase of TiO_2 [21].

The average crystallite size was calculated using the Scherrer formula [6, 25]:

$$D = \frac{K\lambda}{\beta cos\theta} \tag{3}$$

where D is the average crystallite size, K is the Debye-Scherrer constant, λ is the wavelength of CuKα radiation equal to 0.15406 nm, β is the full width at half maximum (FWHM) of the peak, and θ is the Bragg angle.

Five peaks corresponding to different crystallographic planes were selected for the calculation, and β values (FWHM) were measured for each. The crystallite sizes of TiO_2 were approximately 44.36 nm at the 2θ = 25.36° peak, 30.93 nm at 2θ = 38.63°, 18.15 nm at 2θ = 48.13°, 25.02 nm at 2θ = 55.16°, and 17.21 nm at 2θ = 70.41°. Therefore, the average crystallite size of TiO_2, calculated as the arithmetic mean, was approximately 28 nm.

Structural Analysis by Raman Scattering

The structure of the resulting film was investigated using an InVia Raman spectrometer with a resolution ≤ 0.5 cm^{-1} in the visible range. The Raman scattering spectra of the deposited TiO_2 film, presented in Figure 3, show well-defined peaks at frequencies of 143, 194, 392, 514, and 637 cm^{-1}. These bands were identified through factor group analysis. It is known that the Raman spectrum of the anatase phase of TiO_2 contains six active modes with peaks at 144, 194, 397, 517, 513, and 639 cm^{-1} [26, 27], corresponding to the symmetries 1A1g, 2B1g, and 3Eg.

The peaks at frequencies 143, 194, and 637 cm^{-1} are associated with the Eg phonon modes, while the peak at 394 cm^{-1} corresponds to the B1g mode. The Raman line at 514 cm^{-1} represents a doublet composed of vibrational modes A1g and B1g [28]. For the rutile phase, four active Raman modes with symmetries B1g, Eg, A1g, and B2g are typically observed at frequencies 144, 243, 447, and 612 cm^{-1}. Based on the data from [26-28], it can be concluded that the Raman spectrum confirms that the crystalline structure of the film is the anatase polymorph of TiO_2.

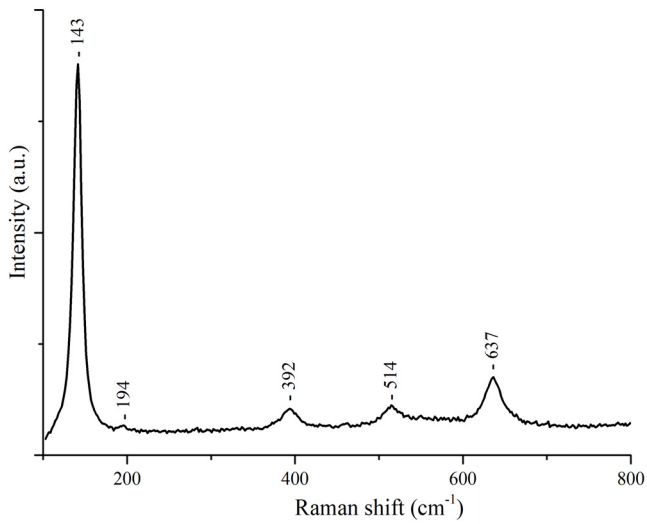

Figure 3. Raman scattering spectrum of the TiO_2 film, showing characteristic peaks of the anatase phase at frequencies of 143, 194, 392, 514, and 637 cm^{-1}

Optical Absorption Spectrum Analysis of the Film

The absorption spectra in the range of 200-1000 nm were investigated using a Shimadzu UV-3600i Plus spectrometer. The absorption coefficient was calculated for the 1500 nm thick film based on the Bouguer-Lambert-Beer law using the following formula:

$$\alpha = \frac{2.303A(\lambda)}{d} \tag{4}$$

where A(λ) is the absorption value corresponding to the wavelength, and d is the film thickness in centimeters.

Figure 4 presents the spectrum of the calculated absorption coefficient, which shows that the film absorbs in the ultraviolet range and is transparent in the visible range. A sharp decline in the absorption coefficient begins around 350-400 nm, corresponding to the material's intrinsic absorption edge. The absorption edge exhibits an exponential dependence on photon energy, indicating a high Urbach energy level. According to [29, 30], this may suggest that the film is a polycrystal with randomly oriented grains. This phenomenon can be explained by the Volmer-Weber crystallization mechanism during the film formation on the substrate, likely due to the lack of chemical bonding between the precursors and the substrate at the initial stage of the process. It could also be a result of quantum size effects caused

by the nanoscale structure. Furthermore, the increase in Urbach energy in such films is often associated with the formation of oxygen vacancies and other defects, which leads to the broadening of absorption tails and a decrease in the crystallinity of the material [31, 32].

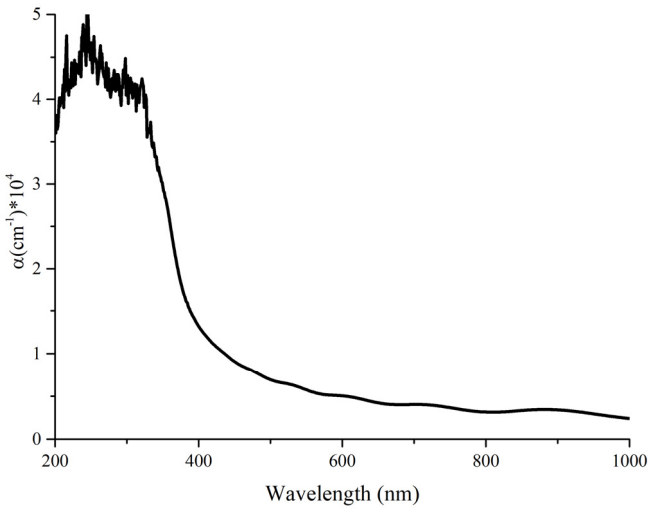

Figure 4. Absorption coefficient of the TiO_2 film in the 200–1000 nm range

The optical bandgap was determined using the Tauc function [19, 29, 30], based on the obtained absorption coefficient α using the following expression:

$$(\alpha h\nu)^n = A\,(h\nu - Eg) \tag{5}$$

where A is a material-dependent constant, Eg is the bandgap energy of the semiconductor, hν is the photon energy, and n is a variable that can take different values depending on the type of electronic transition. Specifically, for an allowed indirect transition, n=1/2, and for an allowed direct transition n=2 [29].

For nanostructured TiO_2 films and nanoparticles, both direct and indirect transitions are possible, which can be explained by their quantum confinement effects and altered electronic structure compared to macroscopic samples. Depending on the size of the nanoparticles and their crystalline structure, an increase or decrease in the bandgap width can be observed, which may be associated, for instance, with the appearance of defects such as oxygen vacancies in the TiO_2 crystallite structure.

The extrapolation of the linear segments of the $(\alpha h\nu)^n$ curves to their intersection with the abscissa (Figure 5) allowed us to estimate the indirect bandgap as 2.3 eV and the direct bandgap as 3.2 eV. Therefore, the presence of linear segments for both transitions indicates that the absorption edge in the TiO_2 film is formed by both direct and indirect allowed interband transitions.

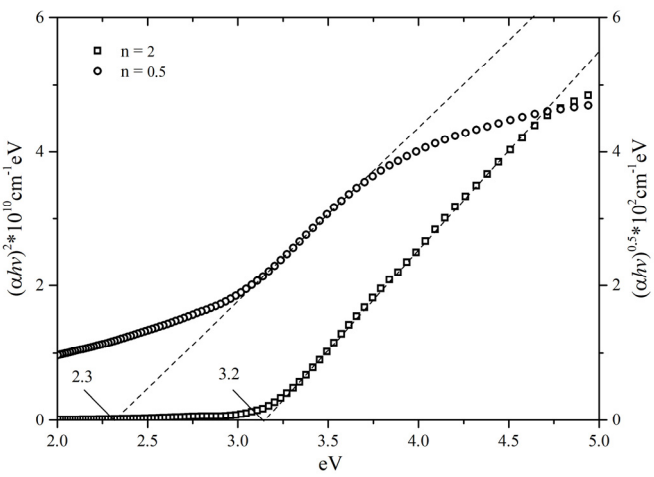

Figure 5. Determination of the bandgap width in the studied film. The square symbols represent the Tauc plot for direct interband transitions, while the circular symbols indicate the plot for indirect transitions.

CONCLUSION

The structural analysis results obtained through XRD and Raman spectroscopy confirm that titanium dioxide films crystallize in the anatase polymorphic phase under thermal ALD conditions. The films exhibit a nanocrystalline structure

with an average crystallite size of approximately 28 nm, as determined from the XRD data. Raman spectroscopy further revealed phonon modes characteristic of anatase, thereby verifying the presence of this phase within the films. The exponential shape observed at the absorption edge suggests a degree of structural disorder, leading to an increase in the Urbach energy. This behavior can be attributed to the Volmer-Weber crystallization mechanism, which is typically associated with the formation of nanocrystalline films, where nucleation occurs predominantly on the surface with limited substrate interaction. The observed bandgap width was slightly smaller than values reported in the literature, indicating the presence of oxygen vacancies within the film's structure. While the widening of the bandgap with decreasing nanoparticle size is typically linked to quantum confinement effects that constrain electron and hole movement, increasing the transition energy between the valence and conduction bands, in this case, the observed reduction in bandgap width suggests that oxygen vacancies have a substantial impact on the film's optical properties, altering the transition energy and offsetting the quantum confinement effects.

Acknowledgments

The authors gratefully acknowledge the financial and technical support provided by the Ministry of Higher Education, Science, and Innovation under project number IL-5421101842

ORCID

Temur K. Turdaliev, https://orcid.org/0000-0002-0732-9357

REFERENCES

[1] A. Garzon-Roman, C. Zúñiga-Islas, and D.H. Cuate-Gomez, Silicon, **16**, 61 (2024). https://doi.org/10.1007/s12633-023-02652-8
[2] A. Garzon-Roman, C. Zúñiga-Islas, D.H. Cuate-Gomez, and A. Heredia-Jimenez, Sens. Actuators A: Phys. **349**, 114064 (2023). https://doi.org/10.1016/j.sna.2022.114064
[3] V. Morgunov, S. Lytovchenko, V. Chyshkala, D. Riabchykov, and D. Matviienko, East Eur. J. Phys. (4), 18 (2021), https://doi.org/10.26565/2312-4334-2021-4-02
[4] D. Li, H. Song, X. Meng, T. Shen, J. Sun, W. Han, and X. Wang, Nanomaterials, **10**, 546 (2020). https://doi.org/10.3390/nano10030546
[5] A. Soussi, A. Ait Hssi, and M. Boujnah, J. Electron. Mater. **50**, 4497 (2021). https://doi.org/10.1007/s11664-021-08976-8
[6] Y. R. Park and K. J. Kim, Thin Solid Films, **484**, 34 (2005). https://doi.org/10.1016/j.tsf.2005.01.039
[7] P. Makuła, M. Pacia, and W. Macyk, J. Phys. Chem. Lett. **9**, 6814 (2018). https://doi.org/10.1021/acs.jpclett.8b02892
[8] W.A.A. Garhoom, and Z. Al Shadidi, East Eur. J. Phys. (4), 164 (2021). https://doi.org/10.26565/2312-4334-2021-4-22
[9] H. Al Dmour, East Eur. J. Phys. (3), 555 (2023). https://doi.org/10.26565/2312-4334-2023-3-65
[10] Y. Wei, Q. Wu, H. Meng, Y. Zhang, and C. Cao, RSC Advances, **13**(30), 20584-20597 (2023). https://doi.org/10.1039/D2RA07839B
[11] C. He, J. He, S. Cui, X. Fan, S. Li, Y. Yang, X. Tan, *et al*., Nanomaterials, **13**(24), 3123 (2023). https://doi.org/10.3390/nano13243123
[12] D.A. Deen, J.G. Champlain, and S.J. Koester, Appl. Phys. Lett. **103** (7), 073504 (2013). https://doi.org/10.1063/1.4818754
[13] D. Nunes, E. Fortunato, and R. Martins, Discover Materials, **2**, 2 (2022). https://doi.org/10.1007/s43939-022-00023-5
[14] H.-H. Li, G.-J. Yuan, B. Shan, X.-X. Zhang, H.-P. Ma, Y.-Z. Tian, H.-L. Lu, and J. Liu, Nanoscale Research Letters, **14**, 119 (2019). https://doi.org/10.1186/s11671-019-2947-5
[15] I.J. Abdisaidov, S.G. Gulomjanova, I.K. Khudaykulov, and K.B. Ashurov, East Eur. J. Phys. (3), 355-358 (2024). https://doi.org/10.26565/2312-4334-2024-3-41
[16] D. Rafieian, W. Ogieglo, T. Savenije, and R.G.H. Lammertink, AIP Adv. **5**, 097168 (2015). https://doi.org/10.1063/1.4931925
[17] K. Al-Attafi, H.A. Mezher, A.F. Hammadi, A. Al-Keisy, S. Hamzawy, H. Qutaish, and J.H. Kim, Nanomaterials **13**, 1940 (2023). https://doi.org/10.3390/nano13131940
[18] H.Y. He, Res. Chem. Intermed. **36,** 155 (2010). https://doi.org/10.1007/s11164-010-0125-6
[19] T.K. Turdaliev, K.B. Ashurov, and R.K. Ashurov, Journal of Applied Spectroscopy, **91**, (2024). https://doi.org/10.1007/s10812-024-01783-z
[20] M. Aravind, M. Amalanathan, and M.S.M. Mary, SN Appl. Sci. **3**, 409 (2021). https://doi.org/10.1007/s42452-021-04281-5
[21] V. Galstyan, E. Comini, G. Faglia, and G. Sberveglieri, Sensors, **13**, 14813 (2013). https://doi.org/10.3390/s131114813
[22] A.A. Rempel, A.A. Valeeva, A.S. Vokhmintsev, and I.A. Weinstein, Russ. Chem. Rev. **90**, 1397 (2021). https://doi.org/10.1070/RCR4991
[23] J. Jitputti, Y. Suzuki, and S. Yoshikawa, Catal. Commun. **9**, 1265 (2008). https://doi.org/10.1016/j.catcom.2007.11.016
[24] J. Jia, H. Yamamoto, and T. Okajima, Nanoscale Res. Lett. **11**, 324 (2016). https://doi.org/10.1186/s11671-016-1531-5
[25] J. Andújar, T. Theivasanthi, T. Thirugnanasambandan, and M. Alagar, arXiv: Chem. Phys. (2013). https://arxiv.org/pdf/1307.1091
[26] A.E. Maftei, A. Buzatu, G. Damian, N. Buzgar, H.G. Dill, and A.I. Apopei, Minerals, **10**, 988 (2020). https://doi.org/10.3390/min10110988
[27] D. Rajkumar, H. Umamahesvari, and P. Nagaraju, J. Mater. Sci.: Mater. Electron. **34**, 38 (2023). https://doi.org/10.1007/s10854-022-09106-8
[28] O. Frank, M. Zukalova, B. Laskova, J. Kürti, J. Koltai, and L. Kavan, Phys. Chem. Chem. Phys. **14**, 14567 (2012). https://doi.org/10.1039/C2CP42763J
[29] I. Y. Bouderbala, A. Guessoum, and S. Rabhi, Appl. Phys. A, **130**, 205 (2024). https://doi.org/10.1007/s00339-024-07366-1
[30] C.M. Mahajan, JOM, **75**, 448 (2023). https://doi.org/10.1007/s11837-022-05621-5
[31] V.R. Akshay, B. Arun, G. Mandal, and M. Vasundhara, Phys. Chem. Chem. Phys. **21**, 12991 (2019). https://doi.org/10.1039/C9CP01351B
[32] Y. Alaya, R. Souissi, M. Toumi, M. Madani, L. El Mir, N. Bouguila, and S. Alaya, RSC Adv. **13**, 21852 (2023). https://doi.org/10.1039/D3RA02387G

ОПТИЧНІ ХАРАКТЕРИСТИКИ ТА КРИСТАЛІЧНА СТРУКТУРА ТОНКОЇ ПЛІВКИ TiO_2 НА СКЛЯНІЙ ПІДКЛАДЦІ, ВИРОЩЕНОЇ ШЛЯХОМ ОСАДЖЕННЯ АТОМАРНОГО ШАРУ

Темур К. Турдалієв
Інститут іонно-плазмових і лазерних технологій імені Арифова Академії наук Узбекистану
100125, вул. Дурмон Юлі 33, Ташкент, Узбекистан

У цьому дослідженні досліджується формування оптичних властивостей і кристалічної структури тонких плівок TiO_2 товщиною приблизно 1,5 мікрометра, вирощених на скляній підкладці методом атомарного шарового осадження з тетраізопропоксидом титану та водою як попередниками. Рентгенівська дифракція та спектроскопія комбінаційного розсіювання підтвердили, що плівки TiO_2 кристалізуються в поліморфній фазі анатазу. Плівки демонструють нанокристалічну структуру із середнім розміром кристалітів приблизно 28 нанометрів, як встановлено рентгенівськими дифракційними вимірюваннями. Рентгенівська дифракційна картина виявила чіткі піки під кутами 2θ 25,3°, 38,6°, 48,0°, 55,0° і 70,4°, що відповідають (101), (112), (020), (121) і (220) кристалографічних площинах, тоді як спектри КРС демонструють виражені піки при частоти 143, 194, 392, 514 і 637 $см^{-1}$, усі характерні для фази анатазу TiO_2. Метод Таука, застосований до спектрів поглинання тонкої плівки, показав, що вона має пряму заборонену зону 3,2 еВ і непряму заборонену зону 2,3 еВ.

Ключові слова: *тонкі плівки діоксиду титану; атомне шарове осадження; фаза анатазу; рентгенівська дифракція; раманівська спектроскопія; енергія забороненої зони; оптичні властивості; енергія Урбаха; нанокристалічна структура*